Pamukkale Üniversitesi Mühendislik Bilimleri Dergisi

Pamukkale University Journal of Engineering Sciences

Numerical investigation of residual stress formation during swage autofrettage process

Mekanik otofretaj işleminde oluşan kalıntı gerilmelerin sayısal olarak incelenmesi

Doğan BARAN[1], Osman BİCAN[1], Yahya DOĞU[1]*

[1]Department of Mechanical Engineering, Faculty of Engineering and Architecture, Kırıkkale University, Kırıkkale, Türkiye.
198858002@kku.edu.tr, bican@kku.edu.tr, ydogu@kku.edu.tr

Received/Geliş Tarihi: 28.11.2024 Revision/Düzeltme Tarihi: 28.02.2025 doi: 10.5505/pajes.2025.86727
Accepted/Kabul Tarihi: 07.03.2025 Research Article/Araştırma Makalesi

Abstract

Autofrettage is a manufacturing process that induces plastic deformation by applying high internal pressure to thick-walled cylinders, enhancing their fatigue life and pressure-carrying capacity. Among the various autofrettage methods employed in industrial applications, swage and hydraulic autofrettage are particularly prominent in the production of heavy weapon barrels. This study focuses on the numerical calculation of residual stresses developed by the of the swage autofrettage process for a heavy weapon barrel. The analysis is performed using Finite Element Analysis (FEA) software, with a two-dimensional (2D) axisymmetric model applied to simulate the process. For a non-autofrettaged barrel under working pressure, the Von Mises equivalent stress is determined to be 1350.3 MPa. In contrast, for an autofrettaged barrel, the Von Mises stress is calculated as 1122.3 MPa at 63% of the barrel thickness. Given that the yield strength of the barrel material is 1195 MPa, the calculated stress remains below this threshold, indicating the structural integrity of the barrel. This corresponds to a 16.88% reduction in Von Mises equivalent stress because of the autofrettage process. The pushing force required during swage autofrettage is assessed through both numerical and experimental methods. The FEA model estimates the pushing force at 135.58T, while empirical measurements yield 142T. The 4.52% discrepancy between these results falls within acceptable limits, affirming the model's reliability. Overall, the findings demonstrate that the FEA-based numerical approach effectively replicates real-world conditions, providing a robust and accurate assessment of stress distribution and pushing force in heavy weapon barrels subjected to swage autofrettage.

Keywords: Swage Autofrettage, Residual Stress, Finite Element Analysis (FEA), Friction

Öz

Otofretaj, kalın cidarlı silindirlere yüksek iç basınç uygulanarak plastik deformasyon oluşturan, yorulma ömrünü ve basınç taşıma kapasitesini artıran bir üretim yöntemidir. Saha uygulamalarda birçok teknik olmasına rağmen, mekanik ve hidrolik otofretaj işlemi ağır silah namlularının üretiminde özellikle öne çıkmaktadır. Bu çalışma, ağır silah namlusunda mekanik otofretaj işlemi sonucu oluşan artık gerilmelerin sayısal olarak hesaplanmasına odaklanmaktadır. Analiz, İki Boyutlu (2D) eksenel simetrik bir model kullanılarak Sonlu Elemanlar Analizi (SEA) yazılımı ile gerçekleştirilmiştir. Otofretaj uygulanmamış bir namluda çalışma basıncı altında Von Mises eşdeğer gerilmesi 1350,3 MPa olarak hesaplanmıştır. Otofretaj uygulanmış namluda ise, namlu kalınlığının %63'ünde Von Mises gerilmesi 1122,3 MPa olarak belirlenmiştir. Namlu malzemesinin akma dayanımı 1195 MPa olduğundan, hesaplanan gerilme bu sınırın altında kalmakta ve namlunun yapısal bütünlüğü korunmaktadır. Bu durum, otofretaj işlemi sonucunda Von Mises eşdeğer gerilmesinde %16,88'lik bir azalmaya karşılık gelmektedir. Mekanik otofretaj işlemi sırasında gerekli mil kuvveti hem sayısal hem de deneysel yöntemlerle hesaplanmıştır. Mil kuvveti SEA yazılımı ile 135,58 ton olarak hesaplanırken, deneysel ölçümler yaklaşık 142 ton değerini vermektedir. Bu sonuçlar arasındaki %4,52'lik fark, kabul edilebilir sınırlar içinde olup modelin güvenilirliğini doğrulamaktadır. Sonuç olarak, çalışma, SEA tabanlı sayısal yaklaşımın gerçek dünya koşullarını etkili bir şekilde yansıttığını ve mekanik otofretaj işlemi uygulanan ağır silah namlusundaki gerilme dağılımları ile mil kuvvetinin doğru bir şekilde hesaplandığını göstermektedir.

Anahtar kelimeler: Mekanik Otofretaj, Kalıntı Gerilme, Sonlu Elemanlar Analizi (SEA), Sürtünme

1 Introduction

The autofrettage process has been applied to high pressure heavy weapon barrels which are subjected to cyclic and variable loads. During each firing, the barrel undergoes high levels of loading and thermal stress, and fatigue can occur due to the dynamic and variable stress cycles [1]-[4].

Autofrettage is a process that creates plastic deformation by applying high pressure to the inner surface of thick-walled cylinders. This process generates beneficial compressive residual stresses on the inner surface, which partially counteract the tensile stresses that occur during service pressure. This balancing effect reduces stress concentration at crack tips. Meanwhile, the autofrettage process reduces the Stress Intensity Factor (K) by alleviating stress at crack tips. This enhances the material's resistance to crack growth, extends its fatigue life, and makes the structure more durable by increasing the pressure carrying capacity.

Depending on the type of autofrettage load applied, autofrettage methods can be divided into the following types: swage autofrettage, hydraulic autofrettage, thermal autofrettage, explosive autofrettage and rotational autofrettage.

Practical applications of autofrettage are listed below and shown in Figure 1.

1) Heavy weapon barrels [5-8],
2) Automotive common-rail direct injection systems [9],

*Corresponding author/Yazışılan Yazar

3) Cylinders, check valves and cutting valves of waterjet cutting units [10],[11],

4) Storage tanks used in the petrochemical industry [12],[13],

5) Boilers, process reactors and vessels in nuclear power plants [14],[15],

6) High pressure processing in food technology [16].

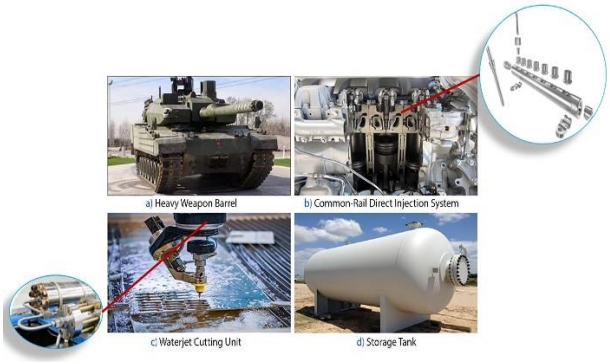

Figure 1. Practical applications of the autofrettage process.

In the autofrettage process, the inner diameter of the thick-walled pressure vessel is exposed to an internal pressure above the working pressure [17]. With the application of pressure, an elastic-plastic transition zone is formed in the cylinder wall (Figure 2). When the autofrettage pressure is removed, the inner diameter of the cylinder undergoes plastic deformation up to the radius of elastic-plastic junction (b). The elastic recovery in the outer diameter of the cylinder compresses the cylinder wall inwards. A beneficial residual compressive stress at the inner wall of the cylinder forms while a residual tensile stress at the outer radius occurs. This residual compressive stress counteracts the secondary tensile stress when working pressure is applied. Thus, the autofrettage process enhances the crack resistance and extends the fatigue life of the weapon barrel.

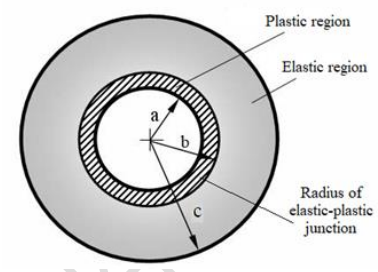

Figure 2. Radius of elastic-plastic junction.

In the defense industry, autofrettage plays a critical role in the production of heavy weapon barrels, significantly enhancing their durability and performance. During repeated firings, the internal surface temperature of barrels can rise to approximately 1100°C due to the combustion of gunpowder, while the maximum internal gas pressure can reach up to 4000 bar [18],[19]. As a result, the autofrettage process is essential for ensuring the structural integrity and longevity of barrels subjected to extreme thermal and pressure conditions.

In practical applications, aside from experimental studies, swage or hydraulic autofrettage is commonly applied to heavy weapon barrels. Typically, hydraulic autofrettage is preferred for barrels with larger diameters, whereas swage autofrettage is more frequently utilized for barrels with smaller diameters. In this study, the stresses that form in the swage autofrettage process are calculated numerically by using the finite element analysis (FEA).

In the swage autofrettage process, a profiled, oversized (extra-large) mandrel plastically deforms the near-bore surface of the gun barrel as it moves axially inside the barrel.

In order to achieve the motion of the mandrel, a force that can overcome the friction force between the barrel and the mandrel is required. Special lubricants are used to reduce the coefficient of friction and the resistance force generated while the mandrel moves through the barrel. In addition, porous phosphate coating (zinc/manganese) on the inner diameter of the barrel and application of stearate-based high pressure lubricants [20] on this coating is the most preferred method in practice.

The swage autofrettage process is distinguished by its simplicity and rapid execution during both the preparation and application stages. But the worst drawback is that the manufacturing tolerances are tight before the process. In addition, it is not possible to apply this process on barrels with variable inner diameter.

Numerous studies in literature have investigated the swage autofrettage process, with key contributions summarized below:

Gibson et al. [6] employed ANSYS FEA software to analyze the plastic deformation mechanisms and calculate residual stress during the swage autofrettage process. The study examined critical parameters such as mandrel slope angle, parallel section length, and friction coefficient. The findings revealed that axial stresses significantly influence residual hoop stresses and contribute to secondary plastic yielding.

Hu and Penumarthy [7] conducted numerical investigations on the swage autofrettage process in thick-walled cylinders using ANSYS FEA. Their analysis incorporated a kinematic hardening material model that accounted for the Bauschinger effect. Numerical results for residual stress at the end of the process were compared with experimental data from the literature. Discrepancies between the two were attributed to specimen preparation errors prior to residual stress measurements. The study further explored the effects of the Bauschinger effect and friction coefficient on stress-strain distributions. Optimal mandrel geometry and Von Mises equivalent stress under working pressure were also determined.

Alinezhad & Bihamta [21] investigated how the modifications on the mandrel geometry affect the residual stresses formed at the end of the swage autofrettage process experimentally and numerically. Experimental results were found to support the numerical results.

Chica et al. [22] focused on parametric analyses related to cold forming, modifying mandrel geometric properties—such as forward and rear slope angles, parallel section length, and percent interference—and examining their effects on residual stresses using ANSYS FEA. The results were compared with numerical studies on swage autofrettage in heavy gun barrels. Additionally, the influence of the outer-to-inner diameter ratio on residual stresses in smaller bore diameters was evaluated.

Hu et al. [23] developed a novel finite element method (FEM) user-programmable function (UPF) incorporating the Bauschinger effect to analyze swage autofrettage in thick-walled cylinders composed of A723 steel. The FEM UPF methodology was validated by replicating uniaxial tension-compression tests on A723 steel. A comparative analysis of this material model with existing models in the literature was

performed. The study highlighted that swage autofrettage produced deeper and more compressive hoop residual stresses on the cylinder's inner surface compared to hydraulic autofrettage. Furthermore, axial stresses were tensile at the end of swage autofrettage but compressive after hydraulic autofrettage. The investigation also demonstrated that chip removal near the inner surface significantly improved stress distributions following swage autofrettage.

The present study numerically calculates stress distributions and pushing forces in a heavy weapon barrel subjected to the swage autofrettage process. The FEA model is developed using ANSYS software, employing a bilinear kinematic hardening material model, plane strain conditions, and the Von Mises yield criterion.

The analysis matrix includes five primary parameters:

- Percent interference
- Barrel material yield strength
- Friction coefficient
- Mandrel parallel section length
- Mandrel slope angle scaling factor

For each parameter, ranges reflective of real-world applications are determined, and their effects on autofrettage are evaluated and compared.

2 Swage autofrettage

Swage autofrettage is performed by forcing a specially manufactured oversized (extra-large) mandrel through the inner diameter of the barrel (Figure 3). The first studies on swage autofrettage are conducted by Davidson et al. [24].

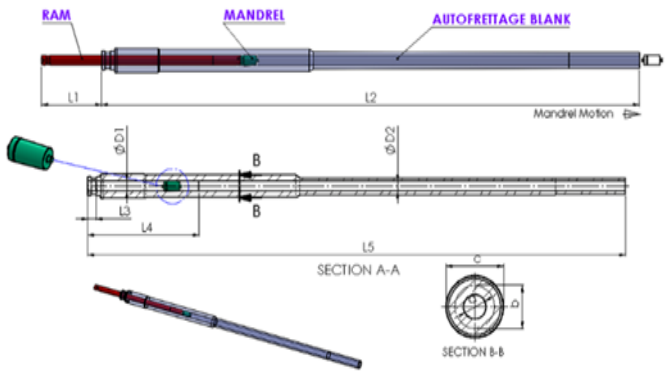

Figure 3. Schematic representation of barrel, mandrel, and ram.

Special machines and equipment are used for swage autofrettage process. It is a critical process to ensure that the oversized mandrel is pushed through the barrel. The mandrel is passed through the barrel using a number of rams according to the barrel length. The hydraulic unit in the machine is used to drive the rams and therefore the mandrel.

Swage autofrettage is mainly more complex in nature from hydraulic. Because, in the swage autofrettage process, remarkably high shear stresses are generated owing to the sliding friction between the mandrel and the barrel during loading stage. In addition, elevated levels of radial and hydrostatic loading in the vicinity of surface distinguish the swage autofrettage process from the hydraulic one [8],[22].

Swage autofrettage mandrels typically involves a parallel section of constant diameter joined by two tapering sections at different slopes (Figure 4). The forward slope of the mandrel is smaller than the rear slope.

The forward and rear tapering sections on the mandrel not only ensure the centering of the mandrel in the barrel, but also plastic deformation and the formation of permanent residual stress.

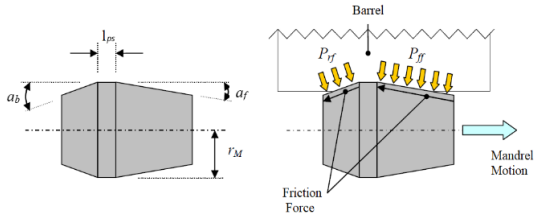

Figure 4. Mandrel diagram [25].

In this study, ANSYS FEA software is used to evaluate stress distributions in the swage autofrettage process. Specification about the barrel and mandrel geometry, material properties and the mesh structure in FEA model are explained in the following subsections.

3 Swage autofrettage numerical calculation: FEA model

There are numerous studies for modelling of the swage autofrettage process in literature. Among these studies, [5], [6],[7],[8],[20],[22],[26] stand out especially. In the literature, it is seen that two-dimensional (2D) axisymmetric models [5], [6],[7],[8],[20],[22],[26] and three-dimensional (3D) quarter-section models [7],[8],[23],[27],[28] are used for swage autofrettage numerical calculations (Figure 5).

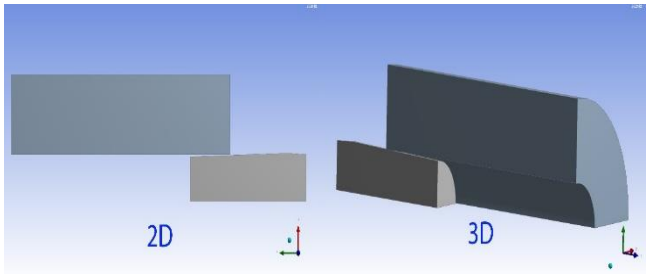

Figure 5. 2D & 3D boundary conditions applied in FEA model.

In this study, a two-dimensional (2D) axisymmetric model is employed for modelling of the swage autofrettage. Given that the process occurs in cylindrical coordinates, the geometric and boundary conditions allow for accurate representation through axisymmetric modeling. This 2D approach not only ensures precise replication of the physical process but also facilitates the use of a finer mesh structure, significantly reducing computational time and enhancing the efficiency of the analysis.

The basic dimensions of the barrel and mandrel in FEA model are shown schematically in Figure 6 [7]. Here, the barrel length (L) is taken as the first 400 mm distance, which is the most critical region where the barrel is exposed to the highest thermal and pressure firing loads. Other dimensions used in the FEA model are given in Figure 6.

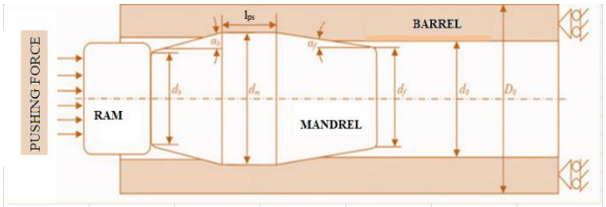

D_0(mm)	d_0 (mm)	L (mm)	d_m (mm)	l_{ps} (mm)	a_f (°)	a_b (°)
Ø315	Ø116	400	Ø119.4	6,35	1,5	3

Figure 6. Geometric dimensions of barrel and mandrel.

The FEA model and its boundary conditions have been created in the ANSYS FEA software are shown in Figure 7. The movement of the A surface of the mandrel in the x direction is constrained; for the movement in the y direction, a displacement of 540 mm is defined for the mandrel to pass through the barrel. The movement of surface B of the barrel in the x direction is allowed and the movement in the y direction is constrained. After the axial movement of the mandrel in the barrel is completed, the 670 MPa working pressure is defined as a boundary condition on the C surface. Working pressure is defined as a 670 MPa, which is the average chamber pressure of heavy weapon barrel [29],[30].

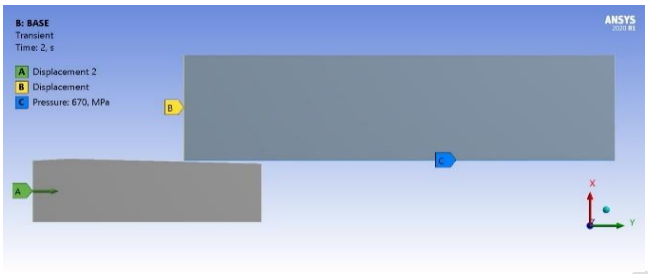

Figure 7. FEA model and boundary conditions.

In the finite element analysis (FEA) software, a bilinear kinematic hardening model (Figure 8) is defined to represent the material behavior. This material model is a base model and includes the Bauschinger effect.

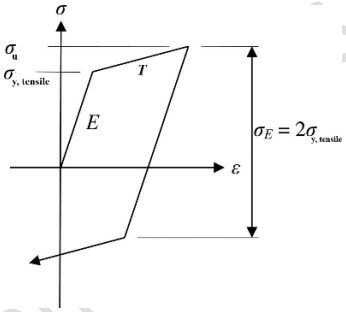

Figure 8. Bilinear kinematic hardening model [31].

The material properties of both the barrel and mandrel are presented in Table 1. The barrel is modeled using AISI 4340 steel, which has a yield strength (σ_y) of 1195 MPa and an ultimate tensile strength (σ_u) of 1332 MPa at a plastic strain of 0.0368. The tangent modulus (T) is calculated as:

$$T = \frac{(1332 - 1195)x10^6}{0.0368} = 3723\ MPa \qquad (1)$$

The mandrel is modeled using tungsten carbide (WC), known for its superior strength and toughness compared to the barrel material [25]

Table 1. Material properties in FEA model.

Barrel		**Mandrel**	
Parameter	**Value**	**Parameter**	**Value**
E (GPa)	200	E (GPa)	500
ϑ	0.3	ϑ	0.24
$\sigma_{y,\ tensile}$ (MPa)	1195	$\sigma_{y,\ tensile}$ (MPa)	-
$\sigma_{y,\ compressive}$ (MPa)	1058	$\sigma_{y,\ compressive}$ (MPa)	
σ_u(MPa)	1332	σ_u(MPa)	
T (MPa)	3723	T (MPa)	-

The literature indicates that the number of elements in the parallel section of the mandrel significantly influences the accuracy of stress distributions [5],[6]. To ensure that the analysis results are independent of element size, a mesh sensitivity study is conducted. The mesh structure for the mandrel's parallel section is formed using element sizes of 2, 4, 6, and 8 mm, corresponding to 5574, 3242, 2850, and 2689 elements, respectively It is determined that the maximum Von Mises equivalent stress under the 670 MPa working pressure has not change significantly depending on the mandrel mesh element size as shown in Figure 9.

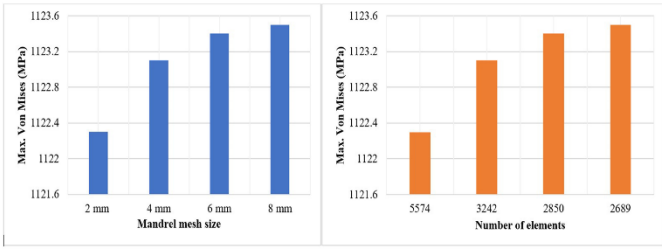

Figure 9. Von Mises equivalent stress versus different element size.

For the mandrel and barrel, mesh structure is formed by using element size of 2 and 4 mm respectively and the resulting mesh structure is shown in Figure 10. The number of nodes/elements for the barrel and mandrel is 17244/5574 in total.

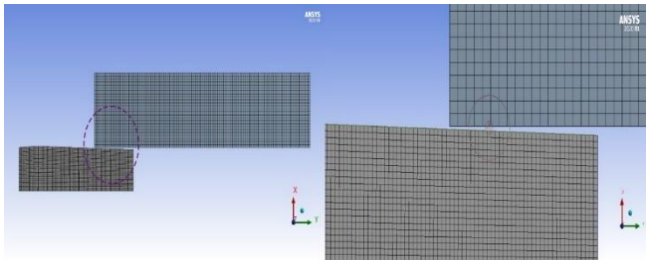

Figure 10. Mesh structure.

The primary objective of this study is to conduct a parametric evaluation of stress distributions in a heavy weapon barrel subjected to the swage autofrettage process using numerical methods. In the investigation, five main parameters (percent interference, yield strength of barrel material, friction coefficient, mandrel parallel section length and mandrel slope angle scaling factor) are considered. The investigation matrix and results are submitted in the following headline.

Table 2. Investigation parameters and their values.

Parameters	Values							
Percent interference (PI)	0.5	1.00	1.5	2.00	**2.94**	3.5		
Yield strength of barrel material (MPa)	1000	1100	**1195**					
Friction coefficient (μ)	0.005	0.010	**0.015**	0.030	0.045	0.060	0.120	0.180
Mandrel parallel section length (l_{ps})	0.25	0.50	0.75	**1.0**	1.50	3.00	4.50	
Mandrel slope angle scaling factor (SF)	0.50	0.67	**1.0**	1.50	2.00	2.50		

4 Results and discussion

In this study, the stresses developing at the barrel with and without autofrettage are calculated numerically. In the swage autofrettage, there are five main parameters affecting the process. As shown in Table 2, the investigation matrix includes five main parameters as listed below:

1) percent interference,
2) yield strength of barrel material,
3) friction coefficient,
4) mandrel parallel section length and
5) mandrel slope angle scaling factor.

The considered wide range and values of each parameter as listed below are determined by considering the practical applications in the field as listed in Table 2.

1) The percent interference is selected as 0.5, 1.0, 1.5, 2.0, 2.94 and 3.5. The percent interference has been determined by fixing the diameter of the parallel section and varying the inner diameter of the barrel.
2) The material yield strengths are selected as 1000 MPa, 1100 MPa and 1195 MPa, determined based on the lower and upper limit depending on the heat treatment process.
3) The friction coefficient is determined by selecting 9 different values: 0.005, 0.010, 0.015, 0.030, 0.045, 0.060, 0.120 and 0.180. These values are the friction coefficients that may occur in case different lubricants are used.
4) Mandrel parallel section length is chosen as 0.25, 0.50, 0.75, 1.5, 3.00 and 4.50 times of the 6.35 mm reference length.
5) The mandrel slope angle scaling factor is selected as 1/2, 2/3, 1.5, 2.0 and 2.5 by scaling reference values (1.5° forward slope angle and 3.0°rear slope angle).

A baseline case is determined in the analyses. The parameters for baseline case are notated as PI: percent interference, σ_y: yield strength of barrel material, μ: friction coefficient, l_{ps}: mandrel parallel section length and SF: mandrel slope angle scaling factor. In Table 2, baseline case values are underlined.

4.1 Analysis matrix

Based on the five main investigation parameters and their values, an analysis matrix in Table 3 is formed in order to systematically represent and evaluate the results in a comparative manner. The analysis matrix includes 30 cases.

A baseline case (Analysis 1) is determined by using reference interference percentage of 2.94, yield strength of barrel material of 1195 MPa, friction coefficient of 0.015, mandrel parallel section length of 6.35 mm and mandrel forward and rear slope angle 1.5° and 3.0°, respectively.

In order to cover the effects of each parameter, analyses are done for all parameter values based on the baseline case. The baseline parameters are selected as the main parameters which are common in the swage autofrettage. Thus, an experimental design methodology was employed in a way that effects of a single parameter are observed at a time based on the baseline case. The full analyses matrix is given in Table 3 by grouping each parameter in the first column. For instance, analyses 1-6 covers the effects of the percent interference.

Autofrettage process requires a certain amount of pressure to be applied to the inner surface of barrel. To calculate the autofrettage pressure (hydrostatic contact pressure, P) between the barrel and mandrel during the swage autofrettage process, certain assumptions and simplifications are required. The autofrettage pressure generated as the mandrel moves axially through the barrel is assumed to exhibit hydrostatic behavior. Thus, equations used in calculating autofrettage pressure for hydraulic autofrettage can be employed. The autofrettage pressure (P) is calculated with the following equation [32].

$$P = \frac{1}{\sqrt{3}}\left[2A\ln\frac{b}{a} + (\sigma_y - A)b^2\left(\frac{1}{a^2} - \frac{1}{b^2}\right) - \sigma_y b^2\left(\frac{1}{c^2} - \frac{1}{a^2}\right)\right] \quad (1)$$

where A is a constant and depends on σ_y, ε_y and T.

The radius of elastic-plastic junction (b) is calculated by using following equation [33].

$$b = a \times e^{\left(\frac{\sqrt{3}P_w}{2\sigma_y}\right)} \quad (2)$$

where a is the barrel inner radius, P_w is the working pressure, and σ_y is the yield strength of the barrel material.

Using these radius values, the corresponding autofrettage pressure is calculated and listed in Table 3.

In this study, the influence of the parameters defined in the investigation matrix on stress distribution is analyzed. The

selection of these parameters is guided by existing literature to assess their impact on stress distribution. The results indicate that the friction coefficient has minimal effect on stress distribution. However, friction force plays a crucial role in determining the pushing force, which is essential for the smooth and safe execution of the swage autofrettage process, ensuring proper mandrel movement within the barrel.

A comparison of the friction coefficients in the investigation matrix reveals that the pushing force varies significantly depending on the boundary conditions. When the lowest friction coefficient (0.005μ) is applied, the pushing force is approximately 9.59 tonnes. In contrast, under the highest friction coefficient (μ), the pushing force reaches 836.17 tonnes. This substantial variation highlights the critical influence of friction coefficient on the swage autofrettage process.

4.2 Comparison of numerical solution for baseline case

First, numeric calculation results are given and compared for the baseline case before evaluating the results for the whole analysis matrix.

The resulting stresses that occur during autofrettage are illustrated in Figure 11, which represents the mid-length position of the tube. In this position, the center of the parallel surface of the mandrel aligns with the tube.

The investigation is first done for the non-autofrettaged barrel under 670 MPa working pressure. Figure 11 illustrates stress distributions in the radial direction for the non-autofrettaged barrel under working pressure for the baseline case. The radial direction is normalized with respect to the inner and outer radius of the barrel in terms of barrel thickness percentage as r*=(r-a)/(b-a)*100. The figure has hoop, radial, axial, and Von Mises stresses obtained from and numerical calculation. The hoop stress reaches its peak value of 884.87 MPa at inner radius; but it asymptotically drops throughout the outer radius to the value of 211.95 MPa. The radial stress varies from -670 MPa (which is the working pressure) to 0 MPa from the inner to the outer radius. Axial stress is exceedingly small, less than 1MPa., due to the nature of stresses developing in thick-walled cylinders. The resulting Von Mises stress is 1350.3 MPa which exceeds the 1195 MPa yield strength. Therefore, it could reduce fatigue resistance, and it may initiate the crack propagation. Therefore, the autofrettage process becomes a need for barrels.

The Von Mises stress under working pressure for the non-autofrettaged barrel is calculated as 1350.3 MPa, exceeding both the yield (1195 MPa) and ultimate tensile strength (1332 MPa) of the barrel material. This raises the question of whether the initial firing pressure could induce an autofrettage-like effect, known as explosive autofrettage. In this process, residual stresses are introduced along the wall thickness of a thick-walled cylinder through high-rate fragmentation explosives. However, since the equivalent stress under working pressure in the non-autofrettaged barrel surpasses the ultimate tensile strength of the material (1332 MPa), no partial plastic zone forms throughout the wall thickness. As a result, the effect of explosive autofrettage is not observed.

Table 3. Analysis matrix.

	Analysis #	Percent Interference (PI)	Yield Strength (MPa)	Friction Coefficient (μ)	Mandrel Parallel Section Length (l_{ps})	Mandrel Slope Angle Scaling Factor (SF)	Autofrettage Pressure (MPa)
Percent Interference (PI)	**1**	**2.94**	**1195**	**0.015**	**1*l_{ps}**	**1**	**1103.2**
	2	0.5	1195	0.015	1*l_{ps}	1	705.95
	3	1.0	1195	0.015	1*l_{ps}	1	869.16
	4	1.5	1195	0.015	1*l_{ps}	1	954.35
	5	2.0	1195	0.015	1*l_{ps}	1	1093.9
	6	3.5	1195	0.015	1*l_{ps}	1	1128.4
Yield Strength (MPa)	**7**	**2.94**	**1195**	**0.015**	**1*l_{ps}**	**1**	**1103.2**
	8	2.94	1100	0.015	1*l_{ps}	1	1015.5
	9	2.94	1000	0.015	1*l_{ps}	1	923.19
Friction Coefficient (μ)	**10**	**2.94**	**1195**	**0.015**	**1*l_{ps}**	**1**	**1103.2**
	11	2.94	1195	0.005	1*l_{ps}	1	1103.2
	12	2.94	1195	0.010	1*l_{ps}	1	1103.2
	13	2.94	1195	0.030	1*l_{ps}	1	1103.2
	14	2.94	1195	0.045	1*l_{ps}	1	1103.2
	15	2.94	1195	0.060	1*l_{ps}	1	1103.2
	16	2.94	1195	0.120	1*l_{ps}	1	1103.2
	17	2.94	1195	0.180	1*l_{ps}	1	1103.2
Parallel Section Length (l_{ps})	**18**	**2.94**	**1195**	**0.015**	**1*l_{ps}**	**1**	**1103.2**
	19	2.94	1195	0.015	0.25*l_{ps}	1	1103.2
	20	2.94	1195	0.015	0.50*l_{ps}	1	1103.2
	21	2.94	1195	0.015	0.75*l_{ps}	1	1103.2
	22	2.94	1195	0.015	1.50*l_{ps}	1	1103.2
	23	2.94	1195	0.015	3.00*l_{ps}	1	1103.2
	24	2.94	1195	0.015	4.50*l_{ps}	1	1103.2
Mandrel Slope Angle Scaling Factor (SF)	**25**	**2.94**	**1195**	**0.015**	**1*l_{ps}**	**1**	**1103.2**
	26	2.94	1195	0.015	1*l_{ps}	0.50	1103.2
	27	2.94	1195	0.015	1*l_{ps}	0.67	1103.2
	28	2.94	1195	0.015	1*l_{ps}	1.50	1103.2
	29	2.94	1195	0.015	1*l_{ps}	2.00	1103.2
	30	2.94	1195	0.015	1*l_{ps}	2.50	1103.2

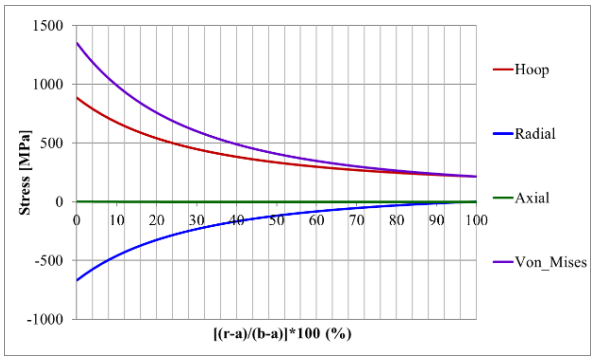

Figure 11. Stress distributions for non-autofrettaged barrel under working pressure for baseline case.

Hoop, radial, axial and Von Mises equivalent stress contours are plotted after the swage autofrettage process along the barrel thickness in Figures 12-15. The stress distributions are plotted as shown in Figure 16 as well.

Hoop stress: A high level of compressive (-) hoop stress occurs at the point of contact between the mandrel and the inner

surface, as shown in Figures 12 and 16. This is due to the combination of forces causing the inner radius of the barrel to expand during the mandrel's movement through the barrel, while the outer radius resists plastic deformation. Conversely, a low tensile hoop stress occurs towards the outer radius. It is observed that the compressive hoop stress reaches -1429.8 MPa at 15% of the barrel thickness. Additionally, tensile hoop stress occurs at 65% of the barrel thickness, with a value of 721.23 MPa.

Radial stress: A compressive radial stress occurs in the contact zone due to moving of the mandrel through the barrel and the expansion of the inner radius as shown in Figures 13 and 16. While radial stress is 0 MPa on both inner and outer radius of barrel, it takes the maximum value of -377.08 MPa at 31% barrel thickness.

Axial stress: Axial stress plays a crucial role in the swage autofrettage process, which is axisymmetric and dynamic, as shown in Figures 14 and 16. During the movement of the mandrel along the barrel, compressing the inner radius, significant compressive (-) axial stress develops near the inner radius due to friction. Conversely, tensile (+) axial stress occurs at the outer radius. At the inner radius, compressive axial stress reaches 733.36 MPa. The axial stress peaks at -889.36 MPa at 2% of the barrel thickness and subsequently decreases through the barrel wall. At 50% of the barrel thickness, the axial stress transitions to the tensile (+) direction, reaching 205.01 MPa at the outer radius.

Von Mises equivalent stress: The Von Mises equivalent stress propagates from the inner radius through the wall thickness by the end of the swage autofrettage process, as illustrated in Figures 15 and 16. This is primarily due to the shift in stress orientation from compressive to tensile. The Von Mises equivalent stress remains constant at approximately 1092 MPa at 15% of the barrel thickness near the inner radius. It then decreases to a minimum value of 192.2 MPa at 33% barrel thickness. After reaching this minimum, the equivalent stress increases, reaching 793.08 MPa at 65% barrel thickness, before decreasing again to 480.65 MPa at the outer radius.

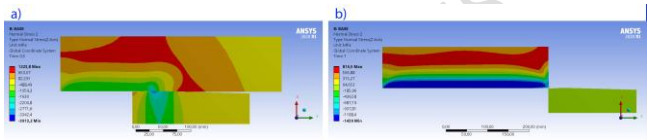

Figure 12. Hoop stress contours during swage autofrettage process a) Mid way, b) Endpoint.

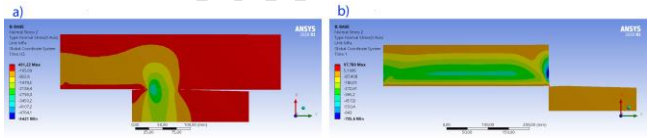

Figure 13. Radial stress contours during swage autofrettage process a) Mid way, b) Endpoint.

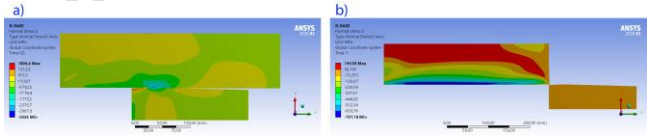

Figure 14. Axial stress contours during swage autofrettage process a) Mid way, b) Endpoint

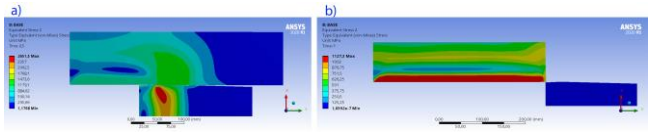

Figure 15. Von Mises stress contours during swage autofrettage process a) Mid way, b) Endpoint.

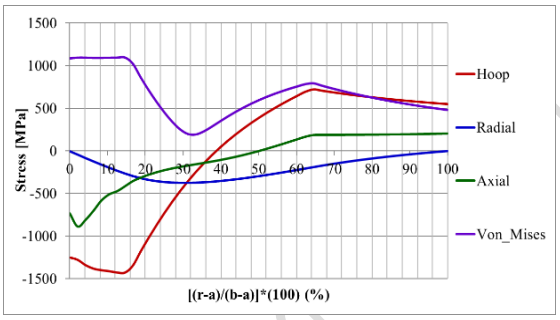

Figure 16. Stress distributions at the end of autofrettage for baseline case.

Hoop, radial, axial and Von Mises equivalent stress contours are plotted under 670 MPa working pressure along the barrel thickness as shown in Figure 17. The stress distributions under 670 MPa working pressure are also plotted as shown in Figure 18.

Hoop stress: After the swage autofrettage, it is seen that the hoop stress has a value of -401.42 MPa at the inner radius and -757.62 MPa at 13% barrel thickness. The most important thing is that the compressive hoop stress is -1007.3 MPa at 65% barrel thickness at the inner radius and its direction is compressive compared to a non-autofrettaged barrel. Thus, the hoop stress is directed to a location far away from the inner radius, which is the critical zone in terms of fatigue and crack initiation.

Radial stress: Due to the effect of the residual stress occurred at barrel thickness, the radial stress reaches its peak value of -666.4 MPa at the inner radius and decreases to 0 MPa at the outer radius.

Axial stress: The axial stress distribution after the swage autofrettage process closely resembles the initial axial stress pattern. At 52% of the barrel thickness, the axial stress transitions to the tensile (+) direction. It reaches a peak value of -760.57 MPa at 2% of the barrel thickness and decreases to a final value of 218.98 MPa at the outer radius.

Von Mises equivalent stress: I The Von Mises equivalent stress propagates through the barrel thickness, showing a significant reduction compared to a non-autofrettaged barrel. The Von Mises equivalent stress is computed at 1122.3 MPa at 63% of the barrel thickness.

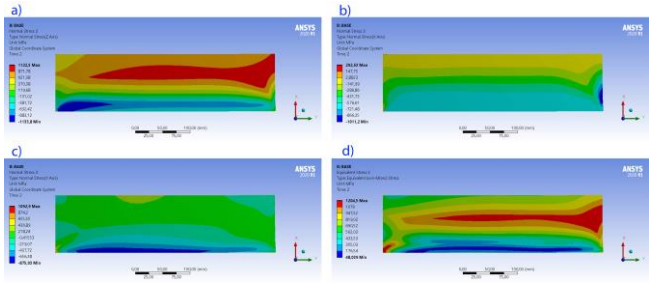

Figure 17. Hoop, radial, axial and Von Mises stress contours for autofrettaged barrel for baseline case.

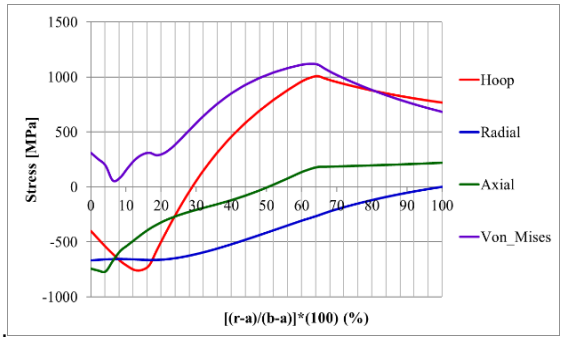

Figure 18. Stress distributions for autofrettaged barrel under working pressure for baseline case.

For comparison, Figure 19 presents the stress distributions for both non-autofrettaged and autofrettaged barrels under the working pressure of 670 MPa in the baseline case. When this pressure is applied to the non-autofrettaged barrel, as shown in Figure 19, the maximum Von Mises stress occurs at the inner radius (1350.3 MPa) and decreases towards the outer radius (211.99 MPa). The maximum stress value of 1350.3 MPa exceeds the yield strength of the barrel material (1195 MPa). In fracture mechanics, the inner radius is considered the critical location for crack initiation and propagation. The equivalent stress exceeding the yield stress at the inner radius presents an unfavorable condition for maintaining the structural integrity of the barrel.

When a working pressure of 670 MPa is applied, the Von Mises equivalent stress fluctuates near the inner radius, reaching its minimum value. At the inner radius, the Von Mises equivalent stress is 310.45 MPa, decreasing to a minimum of 57.15 MPa at 6% of the barrel thickness. Beyond this point, the equivalent stress increases, reaching 1122.3 MPa at 63% of the barrel thickness. This value is below the yield strength of the barrel material (1195 MPa). After peaking, the Von Mises equivalent stress gradually decreases towards the outer radius, reaching 683.78 MPa.

For the autofrettaged barrel, the maximum Von Mises stress occurs at 63% of the barrel thickness, with a value of 1122.3 MPa. In contrast, for the non-autofrettaged barrel, the maximum Von Mises stress reaches 1350.3 MPa at the inner radius. This represents a 16.88% reduction in Von Mises stress for the autofrettaged barrel.

A study [7] conducted on a heavy weapon barrel with similar geometrical dimensions reported an 18% reduction in maximum Von Mises equivalent stress. The results obtained in this study align closely with the values presented in the literature.

As a result, the barrel subjected to the autofrettage process demonstrates a higher pressure-carrying capacity compared to the non-autofrettaged barrel. Pressure-carrying capacity refers to the barrel's ability to withstand applied pressure without undergoing plastic deformation.

Von Mises equivalent stress values for non-autofrettaged and autofrettaged barrels are obtained from numerical calculations under working pressure and summarized in Table 4 for only baseline case. The stress is evaluated at specific locations, including the inner diameter (ID), the elastic-plastic junction radius, and the outer diameter (OD). The table presents data for both post-autofrettage and working conditions, as well as for the non-autofrettaged case.

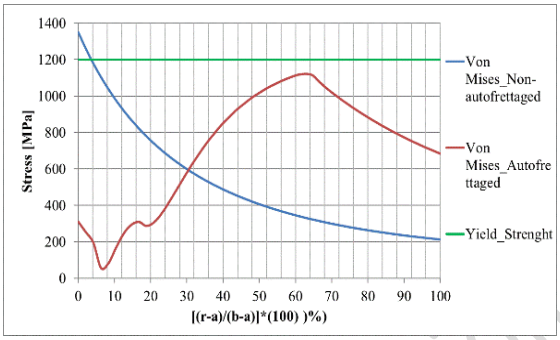

Figure 19. Stress distribution comparison for non-autofrettaged and autofrettaged barrel under working pressure for baseline case.

Table 4. Von Mises stress for non/autofrettaged barrel under working pressure at baseline case.

	Non-autofrettaged (MPa)	Post-autofrettaged (MPa)	Working pressure (MPa)
ID	1350.3	1086.5	310.45
Radius of elastic-plastic junction	-	793.08	1122.3
OD	211.99	793.08	683.78

4.3 Mandrel pushing forces for swage autofrettage process

Swage autofrettage is performed by forcing a specially manufactured oversized (extra-large) mandrel through the inner diameter of the barrel (Figure 3).

Special machines and equipment are used for swage autofrettage process. The mandrel is passed through the barrel using a series of rams for the length of the barrel. The hydraulic unit in the machine is used to drive the rams and therefore the mandrel.

Mandrel pushing force is one of the most critical parameters for swage autofrettage process. Alleviating pushing force means using energy more efficiently. In addition, control of the pushing force will prevent the mandrel from being subjected to more stress and deformation. Therefore, mandrel's life prolongs considerably [5],[7],[26],[34].

The pushing force versus mandrel's position inside the barrel is shown in Figure 20. When the mandrel is placed and travelled inside the barrel, the pushing force swiftly reaches its peak value. Then, the pushing force follows a fluctuating course. Finally, it gradually decreases and drops the zero.

FEA software indicates that with a coefficient of friction of 0.015 μ, the pushing force required from the moment the mandrel's parallel section (l_{ps}) contacts the inner surface of the barrel until the mandrel exits is approximately 1,330,000 N (135.58 tonnes).

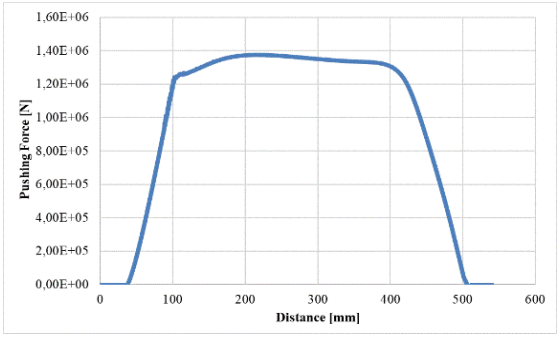

Figure 20. Mandrel pushing force versus barrel distance.

In order to compare the empirical pushing force with the force value calculated by FEA software, LVDT (Linear variable differential transducer) sensors should be used. Within the available possibilities, the pushing force generated during the swage autofrettage process has been read and recorded with a tonnage gauge mounted on the plant (Figure 21). Finally, the pushing force is empirically measured as about 142T.

Figure 21. Tonnage gauge on the swage autofrettage plant.

A comparison between numerical and experimental results reveals a 4.52% error (Table 5). This margin of error is considered reasonable. Furthermore, the numerical study effectively replicates real-world conditions, demonstrating that the FEA boundary conditions are accurately defined.

Table 5. Comparison of numerical and experimental results.

Pushing force(tonnes)	Numerical	Experimental	Error (%)
	135.58	142	4.52

4.4 Parametric analyses

After evaluating numerical results, parametric analyses are performed by using FEA model.

Based on these investigation parameters and their values, an analysis matrix in Table 3 is formed in order to systematically represent and evaluate the results in a comparative manner. The analysis matrix includes 30 cases.

As shown in Table 3, the investigation matrix includes five main parameters:

(1) percent interference,

(2) yield strength of barrel material,

(3) friction coefficient

(4) mandrel parallel section length

(5) mandrel slope angle scaling factor

A wide range of parameter values are determined by considering the applications in the field. By using these five investigation parameters and their values, the analyses matrix given in Table 3 is formed. There are 30 analysis cases. A baseline case (Analysis 1) is determined by using reference interference percentage of 2.94, yield strength of barrel material of 1195 MPa, friction coefficient of 0.015, mandrel parallel section length of 6.35 mm and mandrel forward and rear slope angle 1.5° and 3.0°, respectively. When the effect of each of five parameters is investigated, values of other parameters are kept same as in the baseline case.

At the following subsections, effect of each investigation parameters is given separately.

4.4.1 Percent interference

Stress distribution after the swage autofrettage process is plotted in Figures 22-25 for various barrel diameter as listed in analysis matrix table (Table 3).

The percent interference is selected as 0.5, 1.0, 1.5, 2.0, 2.94 and 3.5. The percent interference (PI) is determined by fixing the diameter of the mandrel's parallel section and varying the inner diameter of the barrel.

The percent interference is shown in Equation 3.

$$\%Interference = \left(\frac{r_m}{a} - 1\right) \times 100 \qquad (3)$$

As shown in Figure 22, hoop stresses transition from compressive near the inner radius to tensile towards the outer radius. It is observed that as the interference percentage increases, the point at which the hoop stress shifts from compressive to tensile moves further along the barrel wall thickness. For 0.5% PI, this transition occurs at 4% of the barrel thickness, while for 3.5% PI, it occurs at 15% of the barrel thickness. The hoop stress at 4% barrel thickness for 0.5% PI is -412.04 MPa, whereas at 15% barrel thickness for 3.5% PI, it reaches -1381.4 MPa.

As plotted in Figure 23, radial stresses are 0 MPa at both the inner and outer radii of the barrel. The radial stress reaches its peak compressive value near the inner radius and increases with higher interference percentages. For 0.5% PI, the radial stress is -385.40 MPa, while for 3.5% PI, it is -38.01 MPa.

Axial stresses are directed from compressive direction near the inner radius to tensile direction towards the outer radius of the barrel similar to the hoop stresses as plotted in Figure 24. Higher interference creates a larger compressive area, which results in a larger axial stress. While the axial stress for 0.5 PI is -272.71 MPa, it is -695.15 MPa for 3.5 PI.

Similar to hoop stresses, axial stresses transition from compressive near the inner radius to tensile towards the outer radius, as shown in Figure 24. Greater interference results in a larger compressive area and higher axial stress values. The axial stress for 0.5% PI is -272.71 MPa, increasing to -695.15 MPa for 3.5% PI.

Finally, as shown in Figure 25, Von Mises equivalent stresses are elevated at both the inner and outer radii. The minimum Von Mises stress is observed at a certain point between the inner and outer radii, corresponding to the shift from compressive to tensile stress. For 0.5% PI, the minimum Von Mises equivalent stress is 336.97 MPa at 4% barrel thickness, whereas for 3.5% PI, it reaches 1078.4 MPa at 15% barrel thickness.

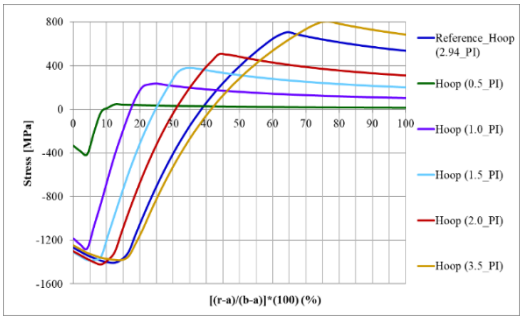

Figure 22. Hoop stress distributions with the respect to diameter.

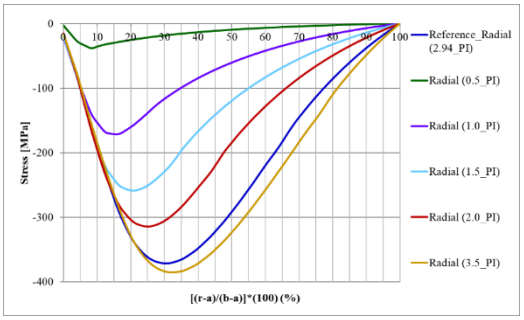

Figure 23. Radial stress distributions with the respect to diameter.

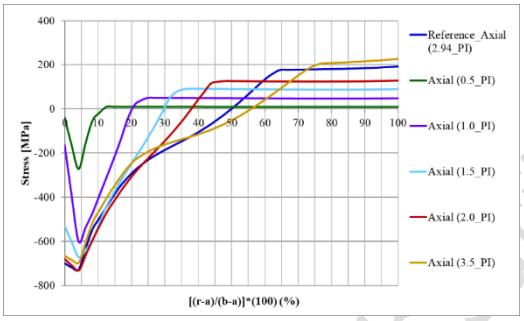

Figure 24. Axial stress distributions with the respect to diameter.

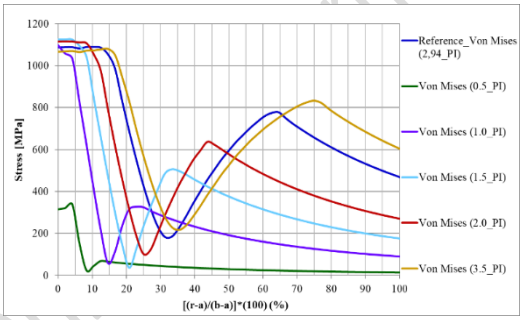

Figure 25. Von Mises stress distributions with the respect to diameter.

4.4.2 Effect of yield strength

The effect of yield strength of barrel material is plotted in Figures 26-29. The barrel material is the AISI 4340 steel. Material yield strength may vary depending on heat treatment process. Analyzes are carried out for the yield strengths of 1000 MPa, 1100 MPa and 1195 MPa, which are within the lower and upper limit values of the barrel material.

The hoop, radial, axial and Von Mises equivalent stress occurred to different yield strengths after swage autofrettage are plotted in Figures 26-29.

When the graphs plotted in Figures 26-29 are evaluated together, the resistance of the barrel material against plastic deformation increased with increasing yield strength. There are findings in the graphs to support this determination at all stress values.

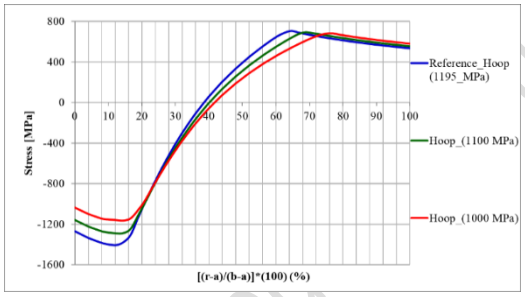

Figure 26. Hoop stress distributions with the respect to yield strength.

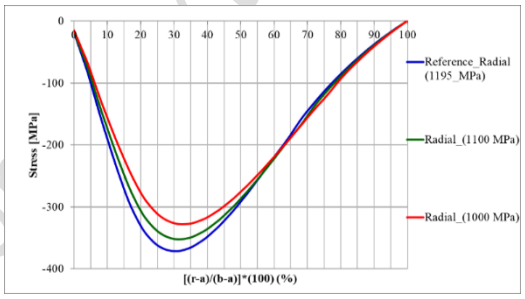

Figure 27. Radial stress distributions with the respect to yield strength.

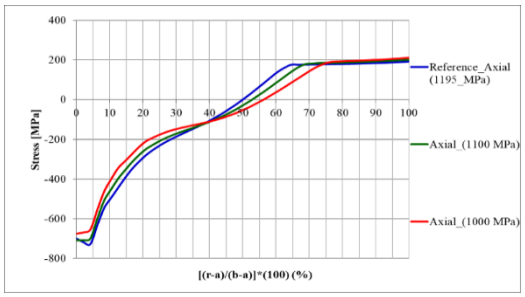

Figure 28. Axial stress distributions with the respect to yield strength.

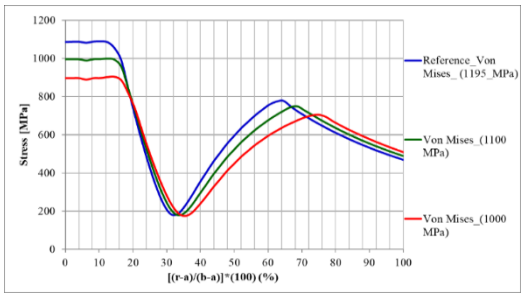

Figure 29. Von Mises stress distributions with the respect to yield strength.

4.4.3 Effect of friction coefficient

The coefficient of friction (μ) is another parameter analyzed in the analysis matrix. As a reference value for the coefficient of

friction, 0.015μ is defined as the boundary condition in the FEA software.

This coefficient of friction of 0.015 is obtained by applying stearate-based oil [20] to the phosphate coating (zinc/manganese) on the inner surface of the barrel.

Many lubricants are used in the swage autofrettage process as stated in the literature [5],[6],[8],[20],[27] It is known that the coefficient of friction values obtained when using these lubricants vary between 0.005 and 0.180μ. In this study, stress distributions for friction coefficients of 0.005, 0.010, 0.015, 0.030, 0.045, 0.060, 0.120 and 0.180μ are plotted.

The hoop, radial, axial and Von Mises equivalent stresses for different friction coefficients after swage autofrettage are plotted in Figures 30-33

It is observed that the hoop and radial stresses are almost similar for all friction coefficients as shown in Figures 30 and 31.

As shown in Figures 30 and 31, hoop and radial stresses exhibit minimal variation across different friction coefficients.

Axial stresses, however, show slight changes with increasing friction coefficients, as shown in Figure 32. When analyzed alongside Figure 30, it is evident that despite variations in the friction coefficient, the contact pressure ($\sigma=\sigma_r$ at $r=r_a$) remains constant, resulting in minimal changes to axial stresses. Additionally, axial stresses become less negative (more positive) as the friction coefficient increases, but the overall trend remains consistent.

Finally, as shown in Figure 33, the Von Mises equivalent stresses are nearly identical across all friction coefficients.

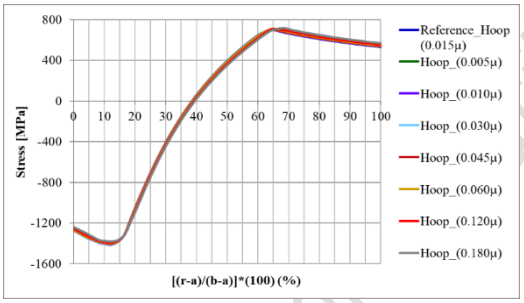

Figure 30. Hoop stress distributions with the respect to friction coefficient.

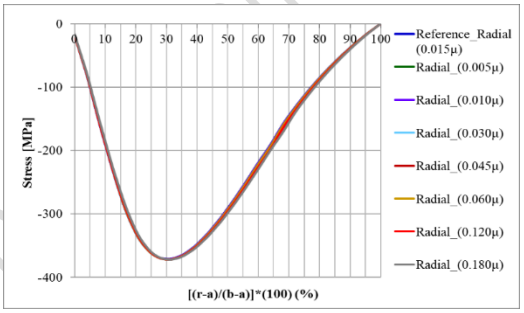

Figure 31. Radial stress distributions with the respect to friction coefficient.

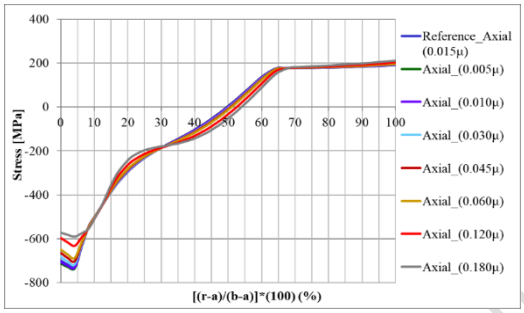

Figure 32. Axial stress distributions with the respect to friction coefficient.

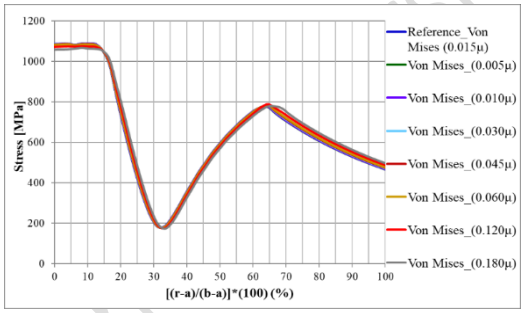

Figure 33. Von Mises stress distributions with the respect to friction coefficient.

4.4.4 Effect of mandrel parallel section length

The effects of mandrel parallel section length on the stress distributions are examined in the analysis matrix. The parallel section length on the mandrel is denoted by the l_{ps}. In the reference study, the value of the l_{ps} is 6.35 mm. Mandrel parallel section length is multiplied by 0.25, 0.50, 0.75, 1.5, 3.00 and 4.50.

The effects of mandrel parallel section length on stress distributions are also examined in the analysis matrix. The parallel section length (l_{ps}) of the mandrel in the reference study is 6.35 mm. This length was varied by multiplying it by factors of 0.25, 0.50, 0.75, 1.5, 3.00, and 4.50.

The hoop, radial, axial and Von Mises equivalent stresses after swage autofrettage for different mandrel parallel section length are plotted in Figures 34-37.

As shown in Figure 34, hoop stresses remain similar across different mandrel geometries, except for l_{ps} values of 3.00 and 4.50 at the end of the swage autofrettage process. In Figure 35, it can be seen that for l_{ps} values of 3.00 and 4.50, axial stresses increase positively at 20% barrel thickness due to compressive axial strain (-). During the swage autofrettage process, larger l_{ps} values lead to plastic axial deformation caused by high shear stresses at the forward and rear tapering sections of the mandrel. Consequently, hoop stress values (Figure 34) decrease significantly for l_{ps} values of 3.00 and 4.50, reducing the overall effectiveness of the swage autofrettage process.

Radial stresses decrease as l_{ps} increases, as shown in Figure 35. This is attributed to the expansion of the plastic deformation zone near the inner radius of the barrel, resulting in lower contact pressure in this region. As a result, the stiffness of the barrel material decreases in the area in contact with the mandrel's parallel section, reducing the radial stress effect.

Axial stresses at the inner radius (Figure 36) are more negative for shorter l_{ps} values, as shorter l_{ps} induces greater compressive axial stresses near the inner radius.

Finally, Differences in radial, axial, and hoop stresses for l_{ps} values of 3.00 and 4.50 significantly influence the Von Mises equivalent stress distributions, as shown in Figure 37.

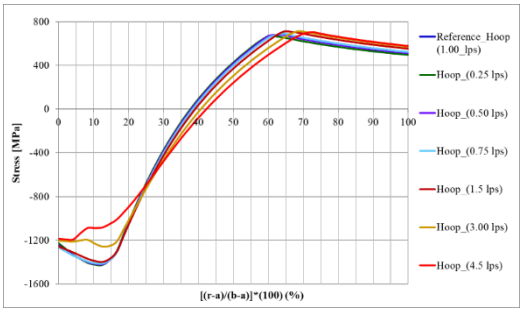

Figure 34. Hoop stress distributions with the respect to mandrel parallel section length.

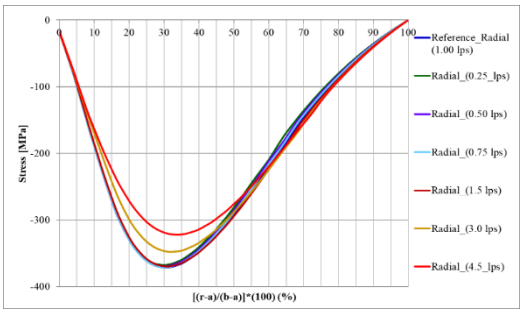

Figure 35. Radial stress distributions with the respect to mandrel parallel section length.

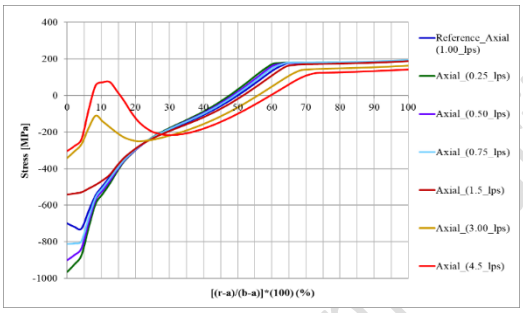

Figure 36. Axial stress distributions with the respect to mandrel parallel section length.

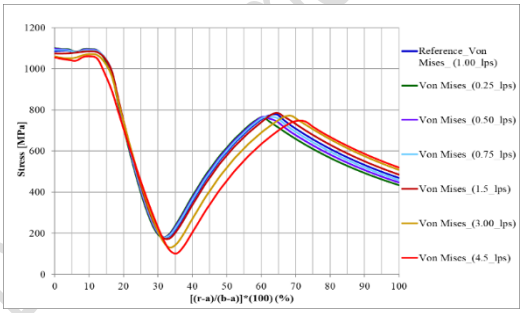

Figure 37. Von Mises stress distributions with the respect to mandrel parallel section length.

4.4.5 Effect of mandrel slope angle scaling factor

The effects of mandrel slope angle scaling factor on the stress distributions are also examined in the analysis matrix.

Mandrel slope angle scaling factor is selected as 1/2, 2/3, 1.5, 2.0 and 2.5 by scaling reference values listed in Table 6 (1.5° forward angle and 3.0°rear slope angle). For example, for a scaling factor of 1/2, the mandrel forward slope angle (a_f) is 0.75° and the rear slope angle (a_b) is 1.5 respectively°.

Table 6. The range of mandrel slope angle scaling factor.

Scaling factor (SF)	Forward slope angle (a_f) (°)	Rear slope angle (a_b) (°)
1/2	0.75	1.5
2/3	1.0	2.0
1	1.5	3.0
1.5	2.25	4.5
2.0	3.0	6.0
2.5	3.75	7.5

The hoop, radial, axial and Von Mises equivalent stresses after swage autofrettage for different mandrel slope angle scaling factor are plotted in Figures 38-41.

As shown in Figure 38, hoop stresses are lower for mandrel geometries with scaling factors of 1/2 and 2/3. In combination with Figure 40, it can be observed that axial stresses play a significant role in reducing hoop stress levels, which directly affect the Von Mises equivalent stress values. Axial stresses are less negative after the swage autofrettage process, limiting the development of hoop stresses for a given equivalent stress (σ_z =the mean of σ_θ and σ_r).

Contact pressure increases as the scaling factor decreases, as shown in Figure 39, leading to higher radial stress at the end of the swage autofrettage process.

Axial stresses at the inner radius show significant variation for lower scaling factors, as shown in Figure 40. Axial deformation occurring during mandrel movement significantly impacts axial stresses after the swage autofrettage process.

Finally, Von Mises equivalent stresses show minimal deviation across different scaling factors, as shown in Figure 41.

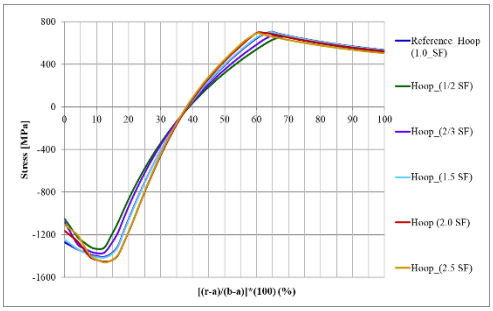

Figure 38. Hoop stress distributions a with the respect to slope angle scaling factor.

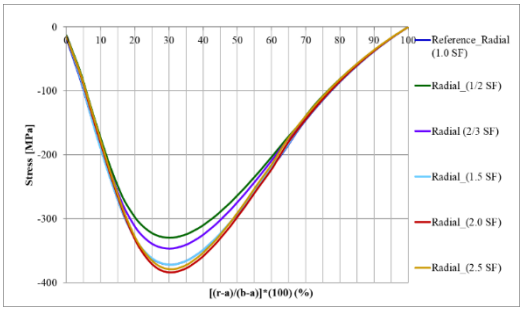

Figure 39. Radial stress distributions with the respect to slope angle scaling factor.

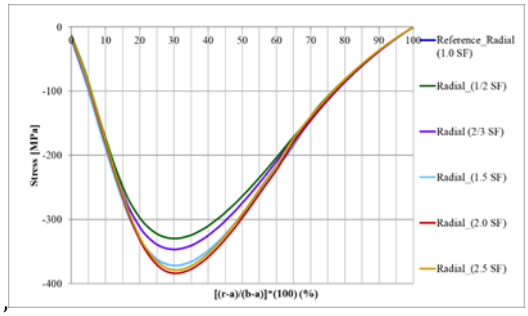

Figure 40. Axial stress distributions with the respect to slope angle scaling factor.

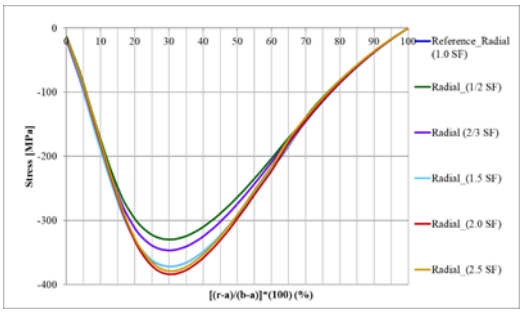

Figure 41. Von Mises stress distributions with the respect to slope angle scaling factor.

4.5 Impact of Bauschinger Effect on the Residual Stress

Theoretically, when the yield stress in the tensile is equal in magnitude to that in compression, there will be no reduction in the yield strength (reverse yielding) until the ratio of outer to inner radius (k) exceeds a value of about 2.2. However, after a critical pressure threshold due to the Bauschinger effect, this phenomenon can also occur at lower ratios of k. In other words, it can take place at lower k values if yielding occurs in compression at a lower stress than in tension due to the Bauschinger effect [24],[35].

The Bauschinger effect is represented by the Bauschinger effect factor. This value, which is defined as the ratio of $\sigma_{y,\,compressive}/\sigma_{y,\,tensile}$, varies between 0.3-1.0 [1]. The lower this factor the lower the yield strength in the compression and Bauschinger effect factor significantly affects the residual stress distribution [32],[37],[38]. In practice, after the autofrettage process, the material is subjected to a low temperature stress relieving process [39] and this negative effect on the residual stress is tried to be eliminated.

If Von Mises residual equivalent stress at the inner radius to be equal to the yield strength in compression ($\sigma_{y,\,compressive}$) of the barrel material after the swage autofrettage, reverse yielding will not take place [40]. In order to prevent reverse yielding after swage autofrettage process:

$$\sqrt{\frac{1}{2}[(\sigma_\theta-\sigma_r)^2+(\sigma_r-\sigma_z)^2+(\sigma_z-\sigma_\theta)^2]}_{r=a} \leq k\sigma_y \quad (4)$$

In this study, the Bauschinger effect factor is calculated as 1058/1195=0.885. The Bauschinger effect factor (k) is assumed to be constant. The plastic strain through the wall thickness is not uniform; therefore, in practice, k varies with the radius [41],[42].

In Table 7, residual equivalent stress results indicate that reverse yielding occurs at the end of the swage autofrettage process for each parameter and its values. Consequently, the stress distribution is adversely affected by the Bauschinger effect. However, further analytical, numerical, and experimental studies are required to thoroughly investigate the implications of this phenomenon.

Table 7. Bauschinger effect on residual stress distribution.

Percent interference (PI)	Residual Von Mises equivalent stress (MPa)	Compressive yield stress (MPa)
2.94	1087.7	1058
0.5	336.97	1058
1.0	1096.6	1058
1.5	1125.2	1058
2.0	1115.2	1058
3.5	1069.1	1058
Yield Strength (MPa)	Residual Von Mises equivalent stress (MPa)	Compressive yield stress (MPa)
1195	1087.7	1058
1100	995.3	1058
1000	896.99	1058
Friction coefficient (μ)	Residual Von Mises equivalent stress (MPa)	Compressive yield stress (MPa)
0.015	1087.7	1058
0.005	1088.4	1058
0.010	1088	1058
0.030	1086.8	1058
0.045	1085.5	1058
0.060	1084	1058
0.120	1076.1	1058
0.180	1068.5	1058
Mandrel parallel section length (l_{ps})	Residual Von Mises equivalent stress (MPa)	Compressive yield stress (MPa)
$1*l_{ps}$	1087.7	1058
$0.25*l_{ps}$	1101.6	1058
$0.50*l_{ps}$	1098.2	1058
$0.75*l_{ps}$	1092.9	1058
$1.50*l_{ps}$	1086.1	1058
$3.00*l_{ps}$	1072.7	1058
$4.50*l_{ps}$	1061.9	1058
Mandrel slope angle scaling factor (SF)	Residual Von Mises equivalent stress (MPa)	Compressive yield stress (MPa)
1	1087.7	1058
0.50	1080.6	1058
0.67	1085.6	1058
1.50	1095.6	1058
2.00	1099.7	1058
2.50	1104.3	1058

5 Conclusion

This study numerically evaluates the stress distributions developed during the swage autofrettage process of a heavy weapon barrel using Finite Element Analysis (FEA). Stress distributions are analyzed based on five key parameters: percent interference, barrel material yield strength, friction coefficient, mandrel parallel section length, and mandrel slope angle scaling factor. Additionally, the pushing force generated during the swage autofrettage process is calculated both numerically and experimentally. The primary findings are summarized as follows:

(1) The Von Mises stress under working pressure for the non-autofrettaged barrel is calculated as 1350.3 MPa, exceeding the yield strength of the material. In contrast, for the autofrettaged barrel, the Von Mises equivalent stress under the same conditions is significantly reduced to 310.45 MPa.

(2) For the autofrettaged barrel, the maximum Von Mises equivalent stress reaches 1122.3 MPa at 63% of the barrel thickness. This value remains below the material's yield strength of 1195 MPa, indicating the structural integrity of the barrel under operational conditions.

(3) The application of autofrettage results in a 16.88% reduction in Von Mises stress compared to the non-autofrettaged barrel under working pressure.

(4) The pushing force required for the swage autofrettage process is calculated numerically at 135.58T using ANSYS FEA software, while experimental measurements yield a force of approximately 142T. The discrepancy between the numerical and experimental results corresponds to an error of 4.52%, which is considered acceptable and within reasonable limits.

(5) Higher percent interference increases compressive residual radial stress throughout the barrel thickness. Concurrently, residual axial stress transitions from compressive near the inner radius to tensile near the outer radius. Greater percent interference also results in larger compressive are, accompanied by higher tensile residual hoop and axial stresses.

(6) Yield strength variations in the barrel material (1000 MPa, 1100 MPa, and 1195 MPa) produce negligible differences in residual stress distributions, suggesting that the autofrettage process is robust across different material strengths

(7) Reducing the friction coefficient between the mandrel and the barrel generally enhances the process efficiency. However, higher friction coefficients lead to slight dissipation of hoop stresses, while axial stresses become less negative (or more positive) due to increased axial loading. Despite this variation, the overall stress distribution trends remain consistent.

(8) The mandrel's parallel section length (l_{ps}) significantly affects axial stress distribution during swage autofrettage. The l_{ps} value of 6.35 mm yields an optimal stress distribution. For larger l_{ps} values (3.00 mm and 4.50 mm), axial stresses increase positively at approximately 20% barrel thickness due to compressive axial strain. Prolonged parallel section lengths induce plastic axial deformation from high shear stresses at the mandrel's forward and rear tapering sections, reducing compressive hoop stress and diminishing the overall effectiveness of the autofrettage process.

(9) The mandrel slope angle scaling factor strongly influences stress distributions. Higher scaling factors (2.0 and 2.5) increase mandrel-barrel contact pressure and reduce plastic deformation, while lower scaling factors (1/2 and 2/3) lead to slight reductions in residual hoop stress. Conversely, residual axial stress near the inner radius becomes significantly more negative as the slope scaling factor increases.

The application of the swage autofrettage process is essential for enhancing the pressure-carrying capacity and longevity of heavy weapon barrels. Numerical analysis of stress distributions provides critical insights into optimizing process parameters, thereby ensuring improved barrel performance and structural reliability.

6 Author contribution statements

In the scope of this study, Author 1 in the literature review, in the conception and design of the study, performing the numerical analysis and writing an article; Author 2 reviewing the article for content and evaluation of obtained results; Author 3 conception and design of the study, reviewing the article for content and assessment of obtained results were contributed.

7 Ethics committee approval and conflict of interest statement

"There is no need to obtain permission from the ethics committee for the article prepared."
"There is no conflict of interest with any person / institution in the article prepared.

8 References

[1] Majzoobi GH, Ghomi A. "Optimization of autofrettage in thick-walled cylinders". *Journal of Achievements in Materials and Manufacturing Engineering,* 16(1-2), 124-131, 2006.

[2] Ali ARM, Ghosh NC, Alam TE. "Optimum design of pressure vessel subjected to autofrettage process". *International Journal of Mechanical and Mechatronics Engineering,* 4(10), 1040-1045, 2010.

[3] Shim WS, Kim JH, Lee YS, Cha KU, Hong SK. "A Study on hydraulic autofrettage of thick-walled cylinders incorporating bauschinger effect". *Experimental Mechanics,* 50, 621-626, 2010.

[4] Bhatnagar RM. "Modelling, validation and design of autofrettage and compound cylinder". *European Journal of Mechanics A/Solids*, 33(2), 94-100, 2005.

[5] Gibson MC, Hameed A, Hetherington JG, "Investigation of driving force variation during swage autofrettage, using finite element analysis". *Journal of Pressure Vessel Technology,* 134(5), 051203, 2012.

[6] Gibson MC, Hameed A, Hetherington JG, "Investigation of residual stress development during swage autofrettage, using finite element analysis". *Journal of Pressure Vessel Technology,* 136(2), 021206-1, 2014.

[7] Hu Z, Penumarthy C. "Computer modeling and optimization of swage autofrettage process of a thick-walled cylinder incorporating Bauschinger effect". *American Journal of Engineering and Applied Sciences,* 3(1), 31-63, 2014.

[8] Hu Z. "Design of two-pass swage autofrettage processes of thick-walled cylinders by computer modeling". *Part C Proceedings of the Institution of Mechanical Engineers, Part C-Journal of Mechanical Engineering Science,* 233(4), 1312-1333, 2019.

[9] Jain A, Khanwelkar S, Saurav SK, Landge A, Yadav U. "Design and performance of hydraulic autofrettage using universal testing machine". *International Journal of Mechanical Engineering Research and Technology,* 6(2), 154-157, 2016.

[10] Trieb F, Schedelmaier J, Poelzl M. "Autofrettage - basic information and practical application on components for waterjet cutting". *Proceedings of WJTA American Waterjet Conference,* United State of America, Houston, Texas, United State of America, 21-23 August 2005.

[11] Çandar H, Filiz H. "Optimum autofrettage pressure for a high pressure cylinder of a waterjet intensifier pump". *Universal Journal of Engineering Science,* 5(3), 44-55, 2017.
[12] A. Partovi A. Analysis of Autofrettaged High Pressure Components, MSc Thesis, Blekinge Institute of Technology, Department of Mechanical Engineering, Department of Mechanical Engineering, Sweden, 2012.
[13] Kamal SM, Dixit US, "Feasibility study of thermal autofrettage of thick-walled cylinders". *Journal of Pressure Vessel Technology,* 137, 061207, 2015.
[14] Majzoobi GH, Ghomi A. "Optimization of compound pressure cylinders". *Journal of Achievements in Materials and Manufacturing Engineering,* 15(1-2), 135-145, 2006.
[15] Malik MA, Knushnood S, Khan M, Rashid B. "Analysis of autofrettaged metal tubes". *15th International Conference on Nuclear Engineering,* Nagoya, Japan, 22-26 April 2007.
[16] Alegre JM, Bravo P, Preciado M. "Design of an autofrettaged high-pressure vessel, considering the Bauschinger effect". *Proceedings of the Institution of Mechanical Engineers Part E-Journal of Process Mechanical Engineering,* 220(1), 7-16, 2006.
[17] Bektaş NB, Altan G, Ergun E, Demirdal G. "İç basınca maruz bir alüminyum diskin elastik-plastik ve artık gerilme analizi". *Pamukkale Üniversitesi Mühendislik Bilimleri Dergisi,* 10(2), 201-206, 2004.
[18] Lawton B. "Temperature and heat transfer at the commencement of rifling a 155 mm gun". *19th International Symposium of Ballistics,* Interlaken, Switzerland, 307-314, 7-11 May 2001.
[19] Putti A, Chopade MR, Chaudhari HE. "A review on gun barrel erosion". *International Journal of Current Engineering and Technology,* 4, 231-235, 2015.
[20] O'hara GP. "Analysis of swage the swage autofrettage process". U.S. Army Armament Research, Development and Engineering Center, Close Combat Armaments Center, Benet Laboratories, Watervliet, New York, United State of America, Report No: ARCCB-TR-92016, 1992.
[21] Alinezhad P, Bihamta R. "A study on the tool geometry effects in the swage autofrettage". *Advanced Materials Research,* 433-440, 2206-221, 2012.
[22] Chica CJ, Marìn MM, Rubio EM, Teti R, Segreto T. "Parametric analysis of the mandrel geometrical data in a cold expansion process of small holes drilled in thick plates". *Materials*, 12(24), 4105, 2019.
[23] Hu Z, Gibson MC, Parker AP. "Swage autofrettage FEA incorporating a user function to model actual Bauschinger effect". *International Journal of Pressure Vessels and Piping,* 191, 104372, 2021.
[24] Davidson TE, Barton CS, Reiner AN, Kendall DP. "New approach to the autofrettage of high-strength cylinders". *Experiment Mechanics*, 2, 33–40, 1963.
[25] Gibson MC. Determination of Residual Stress Distributions in Autofrettaged Thick-Walled Cylinders. PhD Thesis, Department of Engineering Systems and Management, Cranfield University, Defence College of Management and Technology, Cranfield, United Kingdom, 2008.
[26] Iremonger MJ, Kalsi GS. "A numerical study of swage autofrettage". *Journal of Pressure Vessel Technology,* 25(3), 347-351, 2003.
[27] Bihamta R, Movahhedy MR, Mashreghi AR. "A numerical study of swage autofrettage of thick-walled tubes". *Materials and Design*, 28 (3), 804-815, 2007.
[28] Troiano E, Parker AP, Underwood JH, Mossey C. "Experimental data, numerical fit and fatigue life calculations relating to bauschinger effect in high strength armament steels". *Journal of Pressure Vessel Technology,* 125(3), 330-334, 2003.
[29] Kruczynski DL, Hewitt JR. "Temperature compensation techniques and technologies-an overview". U.S. Army Laboratory Command, Ballistic Research Laboratory, Maryland, United State of America, Report No: BRL-TR-3283, 1991.
[30] Makine ve Kimya Endüstrisi Inc. "Product Catalogue". https://www.mke.gov.tr/Kataloglar/Urun-Katalog-Products-Catalogue/2-(21.11.2024).
[31] Abdelsalam O. Analysis and Optimization of Autofrettaged and Shrink-Fitted Compound Cylinders Under Thermo-Mechanical Loads. PhD Thesis, Department of Mechanical and Industrial Engineering, Concordia University, Montreal, Quebec, Canada, 2012.
[32] Çandar H, Filiz H. "Optimum autofrettage pressure for a high pressure cylinder of a waterjet intensifier pump". *Universal Journal of Engineering Science,* 5(3), 44-55, 2017.
[33] Zhu R., Yang J. "Autofrettage of thick cylinders". *International Journal of Pressure Vessels and Piping*, 75, 443-446, 1998.
[34] Perl M, Perry J. "An experimental-numerical determination of the three-dimensional autofrettage residual stress field incorporating bauschinger effects". *Journal of Pressure Vessel Technology,* 128(2), 173-178, 2006.
[35] Perry J. and Perl M. "The effects of the material's exact yield point and its plastic properties on the safe maximum pressure of gun barrels". *Journal of Pressure Vessel Technology,* 139(5), 051401, 2017.
[36] Hill R. *The Mathematical Theory of Plasticity*. New York, USA, Oxford University Press, 1950.
[37] Shim WS, Kim JH, Lee YS, Cha KU, Hong SK. "A Study on hydraulic autofrettage of thick-walled cylinders incorporating bauschinger effect". *Experimental Mechanics*, 50, 621-626, 2010.
[38] Perry J, Perl M. "The effects of the material's exact yield point and its plastic properties on the safe maximum pressure of gun barrels". *Journal of Pressure Vessel Technology,* 139(5), 051401, 2017.
[39] Perl M, Perry J. "The beneficial influence of bauschinger effect mitigation on the barrel's safe maximum pressure". *Journal of Pressure Vessel Technology,* 135(2), 021404, 2013.
[40] Çandar H, Filiz İH. "Experimental study on residual stresses in autofrettaged thick-walled high pressure cylinders". *High Pressure Research,* 37(4), 516–528, 2017.
[41] Parker AP, Underwood JH. "Influence of the bauschinger effect on residual stress and fatigue lifetimes in autofrettaged thick-walled cylinders". U.S. Army Armament Research, Development and Engineering Center, Close Combat Armaments Center, Benet Laboratories, Watervliet, New York, United State of America, Report No: ARCCB-TR-97020, 1997.
[42] Huang XP, Cui WC. "Effect of bauschinger effect and yield criterion on residual stress distribution of autofrettaged tube". *Journal of Pressure Vessel Technology*, 128(2), 212–216, 2006.